Transplantable and functional retinal pigment epithelium derived from non-colony-type monolayer of human induced pluripotent stem cells

Xiaoling Guo
Key laboratory for Rgenerative Medicine, Ministry of Education,Jinan University,Guangzhou ,China
Deliang Zhu
Key Laboratory for Regenerative Medicine, Ministry of Education,Jinan University, Guangzhou,China
Ruiling Lian
Eye Institute,Medical College of Jinan University,Guangzhou ,China
Qiaolang Zeng
Eye Institute,Medical College of Jinan University,Guangzhou,China
Sanjana Mathew
Key Laboratory for Regenerative Medicine,Ministry of Education,Jinan University ,Guangzhou,China
Shibo Tang
Aier School of Opthalmology,Central South University,Changsha,China
Jiansu Chen (chenjiansu2000@163.com)
Eye Institute, Medical College of Jinan University,Guangzhou, China

Research article

Keywords: human induced pluripotent stem cells (hiPSCs), retinal pigment epithelium (RPE), differentiation, spheroid, transplantation

Posted Date: January 27th, 2020

DOI: https://doi.org/10.21203/rs.2.21874/v1

Abstract

Background

Retinal pigment epithelium (RPE) cells derived from human induced pluripotent stem cells (hiPSCs) exhibit great promise in treating retinal degenerative diseases. To develop transplantable and functional hiPSC-RPE cells, here, we used a novel differentiation protocol based on a non-colony-type monolayer (NCM) culture and injectable spheroids.

Methods

The derived hiPSC-RPE cells were identified using reverse transcription-polymerase chain reaction (RT-PCR), immunofluorescence assay, Western blotting, and flow cytometry assay. The functions of transplantable hiPSC-RPE cells in vitro and in vivo were also analyzed by fluorescein leakage test, transepithelial electrical resistance (TEER) assay, atomic force microscopy observation, POS phagocytosis assay, frozen tissue sections, live/dead assay, SA-β-Gal activity assay, and immunocytochemistry.

Results

The derived hiPSC-RPE cells positively expressed biomarkers of RPE cells but not iPSCs, such as CRALBP (97.4%), EMMPRIN (93.8%), Oct4 (2.1%), and Sox2 (2.0%). hiPSC-RPE cells displayed RPE-like characteristics including barrier function, phagocytic activity, and polarized membrane. hiPSC-RPE cell spheroids positively expressed Nestin and exhibited reduced SA-β-Gal staining. Injectable hiPSC-RPE cell spheroids could form monolayers on decellularized corneal matrixes (DCM). After subretinal transplantation for one month, hiPSC-RPE cell spheroids could survive and maintain segmental sheet growth in RPE-degenerated chinchilla rabbits.

Conclusion

This study realized that NCM dissociated hiPSCs were effectively differentiated into transplantable and functional RPE through the sequential addition of defined factors but not involving exogenous genes. This study may lay the foundation for the clinical transplantation of hiPSC-RPE cell spheroids as therapy for RPE degenerative diseases in the future.

Background

Retinal pigment epithelium (RPE) cells are polarized monolayer cells distributed between the choriocapillaris and neural retina. RPE cells play a crucial role in maintaining the function of photoreceptors and the retina [1]. Degeneration or dysfunction of RPE cells is the main cause of retinal diseases including retinitis pigmentosa (RP) and age-related macular degeneration (AMD) [2]. The limited benefit of existing surgical intervention for these diseases has led to increasing interest in the development of approaches to delay RPE cell degeneration [3]. Cell transplantation therapy that

supplements the retina with exogenous RPE cells may halt disease progression. Various cell types have been examined for their utility in RPE cell replacement including ARPE19 cells [4], adult RPE cells [5], fetal RPE cells [6], and many non-RPE cell lines [7–9]. However, sources of donor cells are still very limited and sometimes can cause immunological rejection.

Pluripotent embryonic stem cells (ESCs) are also used as alternative cells for transplantation due to their pluripotency [10, 11]. In 2004, Klimanskaya et al. first reported that putative RPE cells could be derived from spontaneous differentiation of ESCs [12]. Many other studies about RPE cells derived from ESCs can also be found [13–15]. However, the application of ESCs has ethical difficulties as well as immune rejection problems. Adult animal fibroblasts can be reprogrammed into the naive state of ESCs called induced pluripotent stem cells (iPSCs) through forcing the expression of a defined set of transcription factors [16]. There have been previous reports about the generation of human iPSCs [8, 17]. iPSCs can be derived from the patient's own cells, which avoids immune rejection and ethical issues. So far, a number of researchers have reported that iPSCs can be differentiated into RPE-like cells (iPS-RPE) [18–20].

Recently, scientists developed a non-colony type monolayer (NCM) culture method for dissociated cells [21, 22]. The key element in this technology is seeding dissociated cells at high density on Matrigel coating plates in the presence of ROCK inhibitor (Y27632) to facilitate dissociated-cell plating efficiency. One of the advantages of NCM culture is the generation of homogeneous hiPSCs. Chen et al. found that cells under NCM culture showed a more homogeneous response to BMP-4 signaling than WA01 cells in colonies [21]. Our previous study also demonstrated that a half-exchange mTeSR1 medium (HM) culture system that combined Y27632 and high-density dissociated-cell seeding could facilitate the homogeneous growth of hiPSCs [23].

Two approaches to RPE cell transplantation in vivo are predominate: the subretinal injection of a cell suspension or the subretinal insertion of an RPE cell sheet grown in monolayer [24]. However, the survival rate of cell suspension transplantation is relatively low, and the process of cell sheet transplantation is very complex [25, 26].

Huang YC et al. reported that use of the appropriate size of dermal papilla (DP) spheroids could effectively induce hair follicle regeneration and maintain high cell viability when transplanted in vivo [27]. Our previous work also confirmed that spheroid culture could enhance cellular stemness and viability in bovine corneal endothelial cells (B-CECs), corneal stromal cells (CSCs), and human adipose-derived stem cells (ADSCs) [28–30]. We found an interesting phenomenon where B-CEC cell spheroids could disappear and then monolayer cells were able to completely cover either culture plates or decellularized corneal matrix (DCM) in the presence of Y-27632. These research foundations inspired us to generate spheroids of RPE cells derived from human iPSCs (hiPSC-RPE). hiPSC-RPE cell spheroids were generated using agarose microwells, which could be used for scalable production of cell spheroids with a controllable size for cell spheroid transplantation studies.

The polarized monolayer RPE cells have a basal side adherent to the Bruch's membrane (BM), which consists of 2–4 μm acellular extracellular matrix (ECM) complexes among which collagen forms a major

component. The collagenous layer is composed of collagen type I, III, and V fibrils. The collagen grid is embedded in a mass of interacting biomolecules, such as glycosaminoglycans (chondroitin sulfate, dermatan sulfate, and hyaluronic acid) and components of the coagulation and complement system [31]. To better observe the monolayer growth of hiPSC-RPE cell spheroids in vitro, we used DCM as a BM substitute. DCM has a similar structure to BM but the former is more convenient to manipulate and observe. DCM is also comprised of aligned arrays of hydrated type I/V collagen fibrils, glycosaminoglycan, keratin sulfate, and dermatan sulfate [32].

In this study, we examined the potential of dissociated hiPSCs to differentiate into transplantable and functional RPE cells by the sequential addition of defined factors at specific time points. Then, we seeded hiPSC-RPE cell spheroids onto DCM for simulation experiments in vitro. Subretinal transplantation of pluripotent stem cell (PSC)-derived RPE cell suspensions or RPE-containing scaffold sheets have been found to be safe and have rescued vision in animal models and even in patients with retinal degeneration [33–37]. Here, we injected hiPSC-RPE cell spheroids into the subretinal space of chinchilla rabbits with RPE degeneration induced by sodium iodate treatment in vivo. Our study will lay the foundation for the use of hiPSC-RPE cell spheroid transplantation as therapy for RPE degenerative diseases.

Material And Methods

Culture of hiPSCs

The hiPSCs were a gift from the Guangzhou Institutes of Biomedicine and Health, Chinese Academy of Sciences. These hiPSCs were reprogrammed from human umbilical cord mesenchymal cells using methods described in a previous report [38]. hiPSCs were cultured in 1% Matrigel (BD Biosciences, USA) coated dishes at 37 °C, 5% CO_2 and refreshed daily with mTeSR1 medium (StemCell Technologies Inc., Canada). They were passaged once every 6 days with 0.25% EDTA (Sigma, USA) and were then seeded into 6-well dishes at a ratio of 1:6. They were supplemented with 10 μM Y-27632 (Sigma) on the first day of passaging. For generating dissociated hiPSCs, the harvested clonal hiPSCs were pipetted approximately 30–50 times and then were filtered through a 40 μm cell strainer (BD). The dissociated hiPSCs (1×10^6 cells/well) were plated into 6-well dishes. Half-exchange mTeSR1 medium (HM) was used for further culturing of the dissociated hiPSCs based on the non-colony type monolayer (NCM) [23].

Isolation and culture of adult RPE cells

Human eyes were obtained from six male donors after informed consent at the mean age of 45 ± 5 years old. The study was approved by the Human Research and Ethical Committee of Jinan University and the procurement and use of human tissues were in compliance with the Declaration of Helsinki. Human adult RPE cells were isolated and cultured as described in a previous report [39]. Briefly, RPE cells were isolated from the posterior section of the eyeballs using 0.25% EDTA-trypsinase (Gibco, USA) and harvested by centrifugation at 400 × g for 5 min. hRPE cells were cultured in RPE medium that consisted of high-glucose Dulbecco's modified Eagle's medium (HG-DMEM, Gibco), 10% FBS (Gibco), 100 U/mL penicillin

and 100 mg/mL streptomycin (P/S, Gibco) at 37 °C and 5% CO_2. After reaching 100% confluence, the RPE cells were passaged and seeded in 6-well plates with a 1% Matrigel coating (Sigma). The medium containing 100 ng/ml Activin A (R&D Systems, USA) was changed every 3 days.

Differentiation of NCM dissociated hiPSC into RPE cells

The point at which dissociated hiPSCs expanded to 100% confluence in HM was defined as day − 2, and from day − 2 to 0, hiPSCs were cultured in E7 medium without FGF2 but with 10 μM Y-27632. Prior to the beginning of differentiation, dissociated hiPSCs were cultured in proneural medium containing DMEM/F12 (Gibco), 1% nonessential amino acids (NEAA, Invitrogen, USA), and 1% N2 (Invitrogen). From 0–2 days, 10 ng/mL IGF-1 (R&D Systems), 50 ng/mL Noggin (R&D Systems), 10 ng/mL Dkk-1 (R&D Systems), and 10 mM nicotinamide (NIC, Sigma) were added into the proneural medium. From 2–4 days, 10 ng/mL IGF-1, 10 ng/mL Noggin, 10 ng/mL Dkk-1, 10 mM NIC, and 5 ng/mL bFGF were added to the proneural medium. From 4–6 days, 10 ng/mL IGF-1, 10 ng/mL Dkk-1, and 100 ng/mL Activin A were added to the proneural medium. From 6–14 days, 100 ng/mL Activin A and 10 μM SU5402 (EMD Millipore, Germany) were added to the proneural medium. Then, the differentiated cells were mechanically enriched by scraping away cells with non RPE-like (spindle) morphology, and the remaining RPE-like (epithelioid-like) cells were passaged using 0.25% EDTA and seeded into 1% Matrigel coating dishes. From 14–20 days, the enriched cells were cultured in enrichment medium containing HG-DMEM (Gibco), 1% FBS (Gibco), 100 ng/mL Activin A, 1 × sodium pyruvate, and 1 × GlutaMAX (Invitrogen). From 20–30 days, these enriched cells were passaged again as passage 1 (P1) and cultured in RPE medium.

Gene expression analysis

Total RNA from the cells was isolated using a Tissue RNA Miniprep Kit (Biomega, China). The cDNAs were synthesized and used for reverse transcription-polymerase chain reaction (RT-PCR). RT-PCR products were examined after electrophoresis on 2% agarose gels. Gels were scanned for further analysis. For quantification of gene transcripts, cDNAs were first denatured at 95 °C for 3 min, followed by 40 cycles of 95 °C for 10 s and 58 °C for 30 s. The relative expression of the genes was normalized against GAPDH, and quantification was performed using the comparative Ct ($2^{-\Delta\Delta Ct}$) method. The primer sequences are shown in Table 1.

Flow cytometry

Samples were fixed using 4% paraformaldehyde and permeabilized by 0.1% Triton X-100 (Sigma). Then, they were incubated with isotype control or primary antibodies as shown in Table 2 at 4 °C for 30 min. Primary and isotype control antibodies were labeled with fluorophore-conjugated secondary antibodies at 4 °C for 30 min. The labeled samples were detected by a flow cytometry analyzer (BD, USA).

Immunofluorescence assay

An immunofluorescence assay was used to identify the hiPSC-RPE cells as described in a previous report [40]. Briefly, paraformaldehyde fixed cells were permeabilized with 0.1% Triton X-100 and incubated with 3% (w/v) BSA for blocking. Cells were then incubated with primary antibodies as shown in Table 2

overnight at 4 °C. On the second day, the cells were washed twice with PBS and then incubated with FITC-conjugated anti-mouse, FITC-conjugated anti-rabbit, Cy3-conjugated anti-mouse, or Cy3-conjugated anti-rabbit IgG secondary antibodies (1:1000, Bioword, USA) at room temperature for 60 min. Cells were rinsed 3 times with PBS and stained with DAPI (Sigma) before examination by a fluorescence microscope (OLYMPUS, Japan).

Fluorescein leakage test

A fluorescein leakage test (FLT) was used to assess the barrier function of the epithelial cells as described in a previous report [41]. First, 200 μL of cells (1×10^5 cells/mL) were seeded in 6-transwell inserts (Millipore, USA) and incubated at 37 °C and 5% CO_2. After reaching 100% confluence, the cells were fixed with 4% paraformaldehyde and 500 μL of Na-fluorescein solution (10 μg/mL, Sigma) was added into each insert before incubation for the designated time (0, 4, 12, 24, and 36 h) to allow solution leakage into the bottom wells. The values of fluorescein leakage into the wells were measured using a microplate spectrophotometer (VSERSA Max, USA) at 485 nm excitation and 530 nm emission wavelengths. The fluorescein leakage through the inserts without cells was set as 100% (maximum leakage). The fluorescein leakage test (FLT) values were calculated as the amount of fluorescein leakage from hRPE and hiPSC-RPE cells compared to the corresponding maximum leakage.

Transepithelial electrical resistance (TEER) assay

A TEER assay was used to assess the dynamic barrier function of the epithelioid cells [42]. Cells were seeded into 24-transwell inserts at 1×10^4 cells/insert. After reaching 100% confluence on day 7, the dynamic barrier of the cells was determined through measuring TEER across the cell monolayer using Millicell-ERS-2 (Millipore, Temecula, USA). The value of TEER was calculated per the following equation:

$$\text{TEER } (\Omega\ \text{cm}^2) = (R_{total} - R_{insert\ w/o\ Matrigel}) \times A$$

R_{total} is the resistance measured (Ω), $R_{insert\ w/o\ Matrigel}$ (Ω) is the resistance of the insert with or without 1% Matrigel coating, and A is the membrane area (cm^2) of the insert.

Atomic force microscopy observation

Atomic force microscopy (AFM) was used to observe the ultrastructure of cells as described in a previous report [43]. Cells were fixed with 4% paraformaldehyde for 10 min and dried at room temperature before imaging. The curvature radius of the AFM tips was 10 nm. The spring constant was 20–50 N/m with a resonance frequency of 278–317 kHZ. The scanning speed was kept at 0.5 Hz. The ultrastructure of the cells was measured in contact mode. The data analysis was performed using Nanoscope Analysis Software (Thermo Microscopes Proscan Image Processing Software Version 2.1, USA).

POS phagocytosis assay

The photoreceptor outer segment (POS) was isolated as described in a previous report [44]. Briefly, the retinas of porcine eyeballs were collected and agitated in KCl buffer (0.5 mM $CaCl_2$, 1 mM $MgCl_2$, 0.3 M

KCl, and 10 mM HEPES) with 48% w/v sucrose at pH 7.0, and then were centrifuged at 5000 × g for 5 min. The supernatant containing the POS was filtered using sterile gauze, diluted 1:1 with KCl buffer without sucrose, and centrifuged at 4000 × g for 10 min. The isolated POS were then resuspended in 1 mL of PBS and were labeled with FITC (Sigma-Aldrich) at room temperature for 1 h. The labeled FITC-POS were then rinsed and resuspended using HG-DMEM medium with 5% sucrose. Cells were incubated with FITC-POS at 37 °C and 5% CO_2 for 2 h. Last, immunofluorescence was performed using mouse monoclonal antibody ZO-1 and DAPI, and then they were examined under an inverted fluorescence microscope.

Z-stack confocal microscopy polarized membrane observation

Z-stack confocal microscopy was used to observe the polarized membrane of the cells. First, 200 µL of cells (1×10^6 cells/mL) were seeded into 6-well dishes and incubated at 37 °C and 5% CO_2 for 5 days. Immunofluorescence was conducted with the mouse monoclonal antibody ZO-1 and DAPI and the stained cells were examined under a confocal microscope (LSM 510 META; Zeiss, Thornwood, USA).

Western blotting

Cells were washed using cold PBS and lysed using RAPI (Beyotime Biotechnology, China). A total of 50 µg of protein was electrophoresed on 10% SDS-PAGE gels and then transferred to polyvinylidene fluoride membranes (PVDF, Sigma) and blocked using 5% fat-free milk. Then, the membranes were incubated with primary antibodies as shown in Table 2 at 4 °C overnight. The membranes were washed 5 times with TBST and incubated with HRP-conjugated anti-mouse or anti-rabbit IgG secondary antibodies (1:3000, Bioword) at room temperature for 2 h. Bands were visualized with enhanced chemiluminescence (ECL, Pierce, USA).

Production of agarose micro multiwell dishes and hiPSC-RPE cell spheroids

A volume of 500 µL liquid solution of 2% (g/mL) agarose was pipetted into an eighty-one well silicone micro-mold (Micro Tissues Inc., CA, USA). After solidification, the microwell agarose mold was removed using sterilized forceps. The agarose mold was placed in 6-well dishes. Then, 200 µL of cell suspension containing approximately 2×10^5 cells was carefully pipetted into the microwell plate and incubated at 37 °C and 5% CO_2. The medium was changed every 2 days. Cell spheroids (approximately 80 µm diameter, 5×10^3 cells/spheroid) were formed after 3 days.

Preparation of decellularized corneal matrix (DCM)

The lamellar corneal matrix (100 µm thickness) was excised from porcine eyeballs using a microkeratome (Kangming, China) and was rinsed 3 times with PBS. The excised lamellar corneal matrix was treated with 0.25% EDTA-trypsinase (Invitrogen) at 37 °C for 30 min, and then was fixed with 4% paraformaldehyde for 1 day at 4 °C. It was then treated with 0.8% SDS (Sigma) solution at − 80 °C for 30 min and then was transferred to a 37 °C shaking table (350 rpm) for 1 h. It was then rinsed 3 times

with PBS and preserved in 100% glycerol at 4 °C as decellularized corneal matrix (DCM). Before the seeding of cells, the DCM was washed 3 times with PBS containing P/S solution and sterilized under ultraviolet light for 2 h.

Seeding the cell spheroids on the DCM

To test whether cell spheroids in the biomimetic microenvironment could grow well, an in vitro simulation experiment of seeding cell spheroids onto DCM was conducted as described previously [29]. Briefly, cell spheroids were seeded on the DCM. The medium containing 10 μM Y-27632 was changed every 3 days. Viable cell staining with Calcein AM was used for better observation of the cell spheroids on the DCM under a fluorescent microscope. The adherent growing area of the cell spheroid periphery stained by a Live-Dead Cell Staining Kit (Biotium, USA) was measured using ImageJ on days 7 and 14, respectively.

Frozen tissue sections

Tissue samples were mounted using tissue freezing medium (SAKURA Tissue-Tek, USA) and placed at −80 °C until frozen. The frozen tissues were sectioned at a thickness of 15 μm using a cryo-microtome (Thermo Fisher, USA) as described in a previous report [45]. Sections were placed on one side of microscope slides (SAKURA Tissue-Tek, USA). All of the sections were fixed with 4% paraformaldehyde for 15 min. Some sections were incubated for 15 min with DAPI for nuclear staining and examined with an inverted fluorescence microscope. Other sections were used for hematoxylin-eosin (H&E) staining and were imaged using an inverted microscope.

Live/dead assay of Calcein AM and EthD-III double staining

Calcein AM and EthD-III double staining (Molecular Probes, USA) was performed as described in a previous report [23]. Briefly, a standard working solution containing 2 μM Calcein-AM and 4 μM EthD-III was prepared. Cells were incubated with the standard working solution at room temperature for 40 min and were then imaged under an inverted fluorescence microscope.

SA-β-Gal activity assay

SA-β-Gal activity was detected using a Cellular Senescence Assay Kit (Beyotime Biotechnology, China) follow the manufacturer's instructions. We used spheroid or monolayer adherent cells on day 7 and 14 to measure SA-β-Gal activity. Briefly, after reaching 100% confluence, the cells were fixed with 4% paraformaldehyde for 15 min at room temperature and were then incubated in a staining solution overnight at 37 °C. On the next day, the stained cells were washed with PBS and observed under an inverted microscope. A blue color indicated the presence of SA-β-Gal activity. The intensity of the SA-β-Gal activity was calculated using ImageJ software.

Tagging hiPSC-RPE cells with PKH26

The standard protocol was performed as described on the PKH26 Product Information Sheet (MINI2, Sigma). Briefly, a suspension containing 2×10^7 cells was centrifuged (400 × g, 5 min) and washed once using fresh medium without serum. After centrifuging, the cells were resuspended in 1 mL of Diluent C.

Dye Solution (4×10^{-6} M) was prepared by adding 4 μL of PKH26 ethanolic dye solution into 1 mL of Diluent C. Then, 1 mL of Dye Solution was rapidly added to the cell suspension. The final concentration after mixing was 2×10^{-6} M PKH26 with 1×10^{7} cells/well. The mixing suspension was incubated with periodic mixing at room temperature for 5 min. The staining was stopped by adding an equal volume (2 mL) of serum. Then, the suspension was centrifuged at 400 × g for 10 min and washed 3 times. Finally, cells tagged with PKH26 were used for injection.

RPE degeneration chinchilla rabbit model

Rabbits were weighed on an electronic scale and then injected with 1% $NaIO_3$ (40 mg/kg, Sigma) via the ear marginal vein. After one week, the rabbits were injected with 1% $NaIO_3$ (40 mg/kg) again. The next week, they could be used as an RPE degeneration model for cell transplantation.

Preliminary test of hiPSC-RPE cell spheroids in vivo

Animal experiments were approved by the Institutional Animal Care and Use Committee of Jinan University, and animal procedures were conducted following the guidelines of the US National Institutes of Health. Twelve six-month-old chinchilla rabbits with a weight of 1–2 kg were raised in a 12 h dark/light cycle, temperature at 23 ± 2 °C, and relative humidity of 45–55%. Water and food were changed every day. These chinchilla rabbits were randomly separated into four groups: control group (n = 3, 6 eyes), which received no treatment; Na_2IO_3 group (n = 3, 6 eyes), which received Na_2IO_3 treatment; Na_2IO_3 + PBS group (n = 6, 6 right eyes), which received Na_2IO_3 treatment and PBS injection; and the Na_2IO_3 + hiPSC-RPE group (n = 6, 6 left eyes), which received Na_2IO_3 treatment and hiPSC-RPE cell injection. Water containing 210 mg/L cyclosporin A (Sigma) and prednisone were given to these rabbits throughout the experiment to prevent allograft rejection. For PBS or hiPSC-PRE cell injection, the model rabbits were anesthetized with pentobarbital sodium (25 mg/kg, Sigma) and chlorpromazine (5 mg/kg, Sigma). The pupil was dilated using tropicamide (Alcon, Canada) and the eye lid was kept open using a lid speculum. Cell transplantation was performed under a surgical microscope (Ocular Instruments, China) [46]. For subretinal injection, the peritomy was made 2.0 mm posterior to the limbus in the superotemporal quadrant of each eyeball. A sideport knife Beaver blade (BD) was used to make a longitudinal triangular scleral incision starting 2 mm away from the limbus at about the 5° axis toward the choroid until minimal blood reflux appeared. At this point an additional tract through the choroid toward the RPE layer was created using a 30-gauge needle. The hiPSC-RPE cell spheroids labeled with PKH26 were suspended in PBS containing 10 μM Y-27632, and then 10 μL of cell spheroids (approximately 1×10^{5} cells) at a density of 20 cell spheroids/μL were slowly injected through the scleral tunnel using a 50 μL Hamilton blunt syringe with a 30-gauge needle (BD), then the syringe was immediately pulled back.

Immunocytochemistry

Rabbits were sacrificed with an overdose of sodium pentobarbital. Their eyeballs were removed and fixed in 4% paraformaldehyde overnight at 4 °C. Samples were dehydrated with a graded series of ethanol and xylene and subsequently were embedded using paraffin wax [47]. The paraffin sections (5 mm) were cut

and dewaxed in water. After antigen repair, these sections were fixed with 4% paraformaldehyde for 15 min and washed 3 times with PBS. They were permeabilized with 0.1% Triton X-100 for 15 min at room temperature and were blocked with 3% (w/v) BSA (Sigma) at room temperature for 1 h. Then, they were incubated with primary antibodies as shown in Table 2 for 2 h at room temperature followed by FITC-conjugated secondary antibody (1:1000, Bioword) for 1 h at room temperature. These sections were rinsed 3 times with PBS and incubated with DAPI (10 μg/mL) for 15 min. Then, they were examined under an inverted fluorescence microscope.

Statistical analysis

All of the data are presented as the mean ± SEM of at least three separate experiments, and statistical significance was evaluated using one-way ANOVA followed by Tukey's multiple comparison tests. Student's unpaired t-test was used to compare two different groups. $P < 0.05$ was considered statistically significant.

Result

Comparison of NCM dissociated-hiPSCs and clonal hiPSCs

The hiPSCs showed clonal growth and the clones gradually became larger over time. Dissociated hiPSCs in an NCM based-culture could grow well adherently. The dissociated hiPSCs displayed a homogenized cellular state. Immunofluorescence assays demonstrated that both clonal hiPSCs and dissociated hiPSCs were positive for the expression of Nanog, Oct4, Sox2, SSEA4, and TRA-1-60 proteins (Fig. S1A). RT-PCR also showed that the Nanog, Oct4, Sox2, c-Myc, Klf4, Lin28, and Nestin genes were expressed at the mRNA level but the Pax6 gene was not expressed in dissociated hiPSCs and clonal hiPSCs (Fig. S1B). The results of qPCR showed that the mRNA expression levels of Nanog, Sox2, Oct4, c-Myc, Klf4, Lin28, and Nestin had no significant differences between dissociated hiPSCs and clonal hiPSCs (Fig. S1C). The chromosomal stabilities of the dissociated hiPSCs and clonal hiPSCs were detected by karyotype analysis and showed that both maintained a normal 46XX chromosome complement (Fig. S2). These results demonstrated that dissociated hiPSCs and clonal hiPSCs can maintain their undifferentiated characteristics and chromosomal stability.

Differentiation and identification of hiPSC-RPE cells

Because a prerequisite for hiPSC differentiation is shutdown of the self-renewal machinery, dissociated hiPSCs were pretreated in E7 medium without FGF2 for 2 days to encourage spontaneous differentiation. FGF2 withdrawal from the culture medium may promote neuro-ectoderm induction [48], and RPE cells belong to neuro-ectoderm lineages. Therefore, the dissociated hiPSCs were switched into Proneural medium with the sequential addition of defined factors at specific time points. The differentiated cells were mechanically enriched and passaged for further experiments. A schematic illustration of the process is displayed in Fig. 1A.

Both the clonal and dissociated hiPSCs grew very well. The nucleoplasmic relation of the dissociated hiPSCs became lower on day 0 and the epithelial morphology cells began to appear on day 8. The epithelioid-like cell monolayer was formed on day 14. RPE-like (epithelioid-like) cells were mechanically enriched, passaged, and reached 100% confluence on day 20 (Fig. 1B). Immunofluorescence assays were used to characterize the expression of RPE specific biomarkers in the enriched hiPSC-RPE cells (P1). The results showed that the hiPSC-RPE cells strongly expressed CRALBP, Mitf, Tyrosinase, Otx2, EMMPRIN, and RPE-65 (Fig. 1C). RT-PCR showed the expression of RPE-65, EMMPRIN, Otx2, and CRALBP but not that of Nanog, Oct4, Sox2, Klf4, or Lin28 in both the hiPSC-RPE and hRPE cells. In contrast, the hiPSCs expressed Nanog, Oct4, Sox2, and Klf4 but not RPE-65, EMMPRIN, Otx2, or CRALBP (Fig. 1D).

Meanwhile, western blotting showed that the hiPSC-RPE cells also expressed RPE specific proteins such as RPE-65, CRALBP, EMMRPIN, Mitf, Otx2, and Tyrosinase but not Nanog, Oct4, Sox2, or Klf4. This pattern of marker protein expression was opposite to that of the hiPSCs but was similar to that seen in the hRPE cells (Fig. 2A). The examination of representative flow cytometry histograms revealed that hiPSC-RPE cells expressed low levels of Oct4 (2.1%) and Sox2 (2.0%) but expressed high levels of RPE-65 (74.4%), CRALBP (97.4%), Mitf (86.8%), and EMMPRIN (93.8%). These properties were similar to those of hRPE cells, which expressed Oct4 (1.9%), Sox2 (1.7%), RPE-65 (84.2%), CRALBP (100%), Mitf (94.2%), and EMMRPIN (95.2%). The hiPSCs showed high levels of Oct4 (99.9%) and Sox2 (99.9%), but low levels of RPE-65 (4.5%), CRALBP (1.7%), Mitf (0.4%), and EMMRPIN (4.1%) (Fig. 2B).

AFM was used to investigate the topography and deflection error morphologies in 2D and 3D of hiPSC, hiPSC-RPE, and hRPE cells, on the cell surface, and in the cell nucleus. AFM images of hiPSCs in the cells displayed a volcano-like distribution. The cell surface of the hiPSCs was relative rough and the cell nucleus showed an oval shape. AFM images of hiPSC-RPE in the cells revealed a pancake-like configuration, which was similar to that of the hRPE. The cell surface of the hiPSC-RPE was relatively smooth and the cell nucleus displayed a cobblestone-like appearance. The nucleo-cytoplasmic ratio of the hiPSCs was higher than that of the hiPSC-RPE and hRPE (Fig. 2C and S3A). Statistical analysis showed that cell length, width, and height parameters of the hiPSC-RPE cells were similar to those of the hRPE cells ($^{\#}P > 0.05$) but were different from those of the hiPSCs ($^{*}P < 0.05$) (Fig. S3B). At the same time, the cell nucleus length, width, and height parameters of the hiPSC-RPE cells were similar to those of the hRPE cells ($^{\#}P > 0.05$) but were different from those of the hiPSCs ($^{*}P < 0.05$) (Fig. S3C).

Taken together, these results illustrated that our protocol is able to efficiently differentiate hiPSCs into RPE-like cells and that the morphology of the hiPSC-RPE cells was similar to that of the hRPE cells but was different from that of the hiPSCs.

Maintenance of native RPE function in hiPSC-RPE cells

One of the most important properties of RPE cells is a barrier function created by tight junctions. Tight junctions encircle each cell to form an occluding seal monolayer that retards diffusion across the paracellular space [49]. Cytoplasmic anchor protein ZO-1 is often used to establish tight junctions. Z-stack confocal microscopy revealed that ZO-1 showed strong expression on the apical side of both hRPE

and hiPSC-RPE cells (Fig. 3A). This polarized expression of ZO-1 is in accordance with previous reports [39, 50].

An essential function of RPE cells is the phagocytosis of outer segments shed from photoreceptors. To test whether hiPSC-RPE cells had phagocytosis function, both hRPE and hiPSC-RPE cells were incubated with FITC-POS, fixed, and then stained for ZO-1. The results showed that FITC-POS particles were specifically engulfed by cells and extensively distributed into the cytoplasm of hiPSC-RPE and hRPE cells (Fig. 3B), indicating that these cells were capable of phagocytosis. Fluorescein leakage test (FLT) results showed that hiPSC-RPE cells had similar FLT values with hRPE cells at 4, 12, 24, and 36 h (Fig. 3C).

In addition, a transepithelial electrical resistance (TEER) assay was conducted to assess the barrier behavior of the hRPE and hiPSC-RPE cells. The data showed that the value of TEER in hRPE is 129.31.4 Ω cm2 and in hiPSC-RPE it is 127.11.1 Ω cm^2, but there was no significant difference between them ($^{\#}P > 0.05$) (Fig. 3D).

Taken together, these results demonstrated that hiPSC-RPE cells had RPE-like functions such as forming a barrier, phagocytic activity, and a polarized membrane.

Seeding of hiPSC-RPE cell spheroids in vitro

To determine whether hiPSC-RPE cell spheroids remained viable after in vivo transplantation, we performed in vitro simulation experiments in which hiPSC-RPE cell spheroids were seeded on DCM. The porcine lamellar corneal matrix (100 μm thickness) was produced using a microkeratome (Fig. S4A). The frozen DCM and normal cornea (control) were cut to obtain tissue sections for DAPI and H&E staining. The results showed that the DCM had almost no cells in it, but the control cornea had many cells in the epithelial and stroma layers (Fig. S4B).

3D agarose molds containing eighty-one wells were produced using silicone concave microwells. These molds were used to generate hiPSC-RPE cell spheroids (Fig. S4C). The hiPSC-RPE cell spheroids were harvested and seeded onto the DCM. Inverted light microscopy imaging showed that proliferating epithelial-like hiPSC-RPE cells could migrate from the periphery of the adherent spheroids. On day 14, the hiPSC-RPE cell spheroids had disappeared and instead formed an epithelioid-like monolayer that completely covered the DCM (Fig. 4A). A live/dead assay was performed to assess the viability of the hiPSC-RPE cells cultured on the DCM. On day 0, cells in the hiPSC-RPE cell spheroids were viable, shown in green fluorescence by Calcein AM staining. Red fluorescence indicated dead cells by EthD-III staining. After 7 days, the majority of the cells were stained by green fluorescence and a limited number of dead cells were located mainly in the center of the hiPSC-RPE cell spheroids, showing red fluorescence. On day 14, the cell spheroids had disappeared and the remaining monolayer cells were only stained by green fluorescence (Fig. 4B). Meanwhile, double staining in an immunofluorescence assay showed that the monolayer hiPSC-RPE cells cultured on DCM were expressing Occludin, Mitf, ZO-1, and RPE-65 (Fig. 4C).

In addition, the hiPSC-RPE cells were stained by SA-β-Gal to determine the proportion of senescent cells. A blue color indicates the presence of SA-β-Gal activity. Positive staining of SA-β-Gal was detected in

spheroids or conventional cultured hiPSC-RPE cells on days 7 and 14 (Fig. 4D). Statistical analysis of SA-β-Gal activity revealed that the percentages of positive staining cells in spheroid or conventional culture hiPSC-RPE cells were 8.01±0.44% and 22.47±0.75% on day 7, respectively. The senescent cells in the spheroid culture hiPSC-RPE cells were lower at 14.46±0.32% than those in the conventional culture hiPSC-RPE cells ($^{**}P < 0.01$) (Fig. 4E). After 14 days, the cell spheroids had disappeared and there were 15.23±0.61% senescent cells in the spheroid culture hiPSC-RPE cells and 68.68±1.34% in the conventional culture hiPSC-RPE cells. There was a 53.38±0.95% increase in senescence in the conventional culture hiPSC-RPE cells compared with the spheroid culture hiPSC-RPE cells ($^{**}P < 0.01$) (Fig. 4E). Furthermore, western blotting showed that hiPSC-RPE cells in a spheroid culture could express Nestin, which was not expressed in hiPSC-RPE cells in conventional culture (Fig. 4F); Nestin is a neural progenitor cell marker.

In our study, we reported a novel method to produce hiPSC-RPE cell spheroids using agarose multiwell dishes. The hiPSC-RPE cell spheroids are able to maintain an integrated monolayer epithelioid morphology as well as viability after being injected onto DCM. Spheroid culture could enhance the viability of hiPSC-RPE cells, which will lay the foundation for hiPSC-RPE cell spheroid transplantation in vivo.

Preliminary test of hiPSC-RPE cell spheroids in vivo

To track the transplanted cell situation in vivo, hiPSC-RPE cell spheroids were labeled with lipophilic red dye (PKH26), which could display red fluorescence (Fig. S5A). The classical external approach for RPE transplantation was conducted to inject hiPSC-RPE cell spheroids into the upper temporal region of the equator in rabbit eyeballs (Fig. S5B). A schematic of the external approach cell transplantation is shown in Fig. S5C. One month after transplantation, H&E staining showed that the control group had a complete RPE layer, but the RPE layers in the $NaIO_3$ and $NaIO_3$ + PBS groups were almost totally degenerated. A segmental sheet growth RPE layer was observed in the $NaIO_3$ + hiPSC-RPE group (Fig. 5A). An immunocytochemistry assay showed that a specific marker of human cells (AHNA) could not be detected in the control group but was positive in the $NaIO_3$ + hiPSC-RPE group. Meanwhile, cells tagged with PKH26 could not be observed in the control group but could be detected in the $NaIO_3$ + hiPSC-RPE group (Fig. 5E). These results demonstrated that hiPSC-RPE cell spheroids injected into the subretina of RPE degenerated chinchilla rabbits could survive for at least one month and maintain segmental sheet growth.

Discussion

The retina is a sensor and processor of visual information. Retinal damage can cause permanent loss of vision. However, recent studies in regenerative medicine have aroused hope for rescuing visual function. One of the strategies for treatment of retinal diseases is the transplantation of retinal cells, especially RPE. Partial recovery of visual function by replacement of RPE cells has been reported [3, 51, 52].

Due to the limited resources of donor cells, RPE cells derived from stem cells, especially ESCs and iPSCs, are required. In the field of ophthalmology, great progress has been made in research on iPSC differentiation. Currently, iPSCs can be successfully differentiated into corneal epithelial cells (CECs) [53, 54], eye trabecular reticular cells [55], rod cells [56], retinal progenitor cells [57, 58], RPE [59], and so on [37]. Brandl C et al. documented that adult dermal fibroblasts can serve as a valuable resource for iPSC-RPE with characteristics highly reminiscent of RPE cells [60]. Significantly, in 2017, Takahashi et al. first performed iPS-RPE-based autologous cell transplantation for treatment of neovascular AMD in one patient, and no serious adverse events were noted after one year of follow-up [61]. In addition, Westenskow et al. reported that the iPS-RPE grafts remained viable and did not induce any obvious pathological changes [62].

Usually, the process of differentiation of iPSCs into RPE is time consuming and has a low efficiency. The survival rate of transplanted iPSC-RPE cells in vivo is not high [12, 63, 64]. Recently, Buchholz et al. reported that iPSCs induced with a series of small molecules such as IGF-1, Noggin, DKK-1, Nicotinamide, bFGF, Activin A, SU5402, and VIP could be rapidly differentiated into RPE phenotype cells after only 14 days [65]. Additionally, we also found that dissociated hiPSCs-based NCM culture was advantageous in the process of differentiation [66].

In our study, we modified the differentiation method proposed by Buchholz et al. Dissociated hiPSCs based on NCM culture were pretreated with E7 iPS culture medium without bFGF for 2 days to inhibit proliferation and promote differentiation [64]. RPE-like cells began to appear on day 8 and formed a cell monolayer after removal of the dead cells through changing the medium on day 14. Our results showed that the percentage of $CRALBP^{+}$ cells among the hiPSC-RPE could reach 97.4%.

Usually, an RPE subpopulation with divergent morphology can be partially separated by selective trypsinization of calcium-dependent adhesion [67]. In our study, RPE-like cells were digested using 0.25% EDTA instead of trypsin to reduce any damage to their calcium-dependent adhesion. Generally, RPE cells tend to undergo morphological changes post passaging due to epithelial-mesenchymal transition (EMT) [68–70]. The tight junction of cells is vital to maintain epithelial morphology and restrain EMT occurrence [71]. In this study, hiPSC-RPE cells could retain their epithelial morphology and barrier function as shown by Matrigel and Activin-A (MA) treatment based on our previous study [42]. Their morphological features showed that hiPSC-RPE cells were more similar to hRPE cells than hiPSCs. In addition, hiPSC-RPE cells could express ZO-1 in relation to tight junctions. hiPSC-RPE cells had similar functions to hRPE cells in regard to barrier and phagocytosis activity. Taken together, the hiPSC-RPE cells in our study possessed normal morphology and functioned like RPE cells. Kokkinaki et al. also demonstrated that iPS-RPE could exhibit ion transport, membrane potential, and gene expression patterns similar to native RPEs [72].

Recent advances in cell culture research have shown that 3D cultures can bridge the gap between cell culture ex vivo and live tissue in vivo. Cells cultured in a 3D environment could generate many differences in cell behaviors and characteristics compared with that in a conventional 2D environment [73]. Cell-to-cell and cell-to-matrix interactions are maintained, and the stemness of progenitor cells can be enhanced

in a 3D spheroid microenvironment [74]. 3D spheroid cultures can form distinct ECMs and establish new ECM interactions to improve cell viability and influence cell fate [75–77]. Bayoussef et al. documented that spheroid muscle cells exhibited higher proliferative capacity [28].

There are many approaches to generating cell spheroids including centrifugation, pellet culture, hanging drop culture, spinner or rotary dynamic culture systems, and so on [78, 79]. Hanging drop or pipetting cells into multiwell plates are time consuming and laborious approaches. The generation of cell spheroids in a suspension culture in non-adhesive culture vessels results in a lack of homogeneity [78]. Here, we reported a novel method to produce hiPSC-RPE cell spheroids using agarose multiwell dishes. Cell spheroids with a uniform size could be quickly formed at the bottom of the non-adhesive agarose microwells. The agarose multiwell dishes easily allowed for the simultaneous generation of hundreds of homogenous hiPSC-RPE cell spheroids.

The progenies derived from the cell spheroids showed only limited staining for the senescence marker SA-β-Gal, had a regular morphology, and grew at a higher density compared with passaged CECs [80]. Short-term spheroid formation of adipose-derived stem cells (ASCs) before monolayer culture could enhance their properties of stemness, angiogenesis, and chemotaxis. ASCs derived-cell spheroids exhibited higher expansion efficiency with less senescence including SA-β-gal staining and p21 expression [81]. In our study, SA-β-Gal activity assays showed that spheroid cultures could reduce cell senescence in hiPSC-RPE, and hiPSC-RPE cell spheroids could positively express Nestin, which is a major intermediate filament protein of embryonic central nervous system progenitor cells. Expression of “progenitors” marker Nestin revealed a distinct molecular reprogramming of the cells into a stem cell state [82].

An experiment of cell spheroids seeded on the DCM can be used to determine whether cell spheroids remain viable after in vivo transplantation. Huang et al. reported that cells from dermal papilla (DP) spheroids were able to maintain their structural integrity and cellular viability after an in vitro simulation experiment of the injectability of DP spheroids on culture plates [27]. As a natural ECM biomaterial, DCM is easier to obtain and is more suitable for observing cell attachment and migration [29]. Our results showed that hiPSC-RPE cells could migrate from the periphery of adherent cell spheroids and grow into a confluent monolayer over 14 days when incubated with the ROCK inhibitor Y-27632. The hiPSC-RPE cell spheroids maintained high cell viability for transplantation. Y-27632 can enhance cell adhesion, motility, and proliferation of human CEC spheroids [83]. Y-27632 treatment also allowed prostate colony cells to replate efficiently, increased the cloning efficiency of prostate stem cells in a prostate sphere assay, and suppressed cell dissociation induced apoptosis [84]. Our previous study also confirmed that Y-27632 could decrease cell death inside spheroids, enhance cell proliferation in the spheroid periphery, and promote the monolayer growth of injectable B-CEC spheroids.

There are internal and external approaches for subretinal RPE transplantation. Dorey et al. reported that the internal technique was more precise while the external approach consistently resulted in a higher percentage of transplanted cells on Bruch's membrane [85]. Moreover, subretinal injection of hiPSC-RPE

cells by the external approach is relatively easier and safer compared with the internal approach. Thus, we chose subretinal injection of hiPSC-RPE cells through an external approach in vivo study. One month after injection of hiPSC-RPE cell spheroids into the subretinal space of RPE degeneration chinchilla rabbits, a segmental sheet of RPE was observed in the cell transplantation eyeballs. Other studies have shown that mono- and multilayer RPEs could be formed after injection of RPE micro-aggregates into the subretinal space, and apoptotic cells were rarely seen [86]. In contrast to transplantation of dissociated cells, micro-aggregate transplantation developed in small patches in the outer segment of the neural retina, and these transplanted cells could survive and maintain their outer segments over the long-term [87]. Since the subretinal space is an immune-privileged site, the posttransplantation hiPS-RPE spheroids could survive at least one month without systemic immunosuppression in our model, which may also be partially due to the administration of cyclosporin A. In this study, there are still some limitations in that no comparison of the differences between hiPSC-RPE spheroid and hiPSC-RPE suspension transplantation was conducted. In addition, we didn't perform OCT imaging or assess retinal function after hiPSC-RPE spheroid transplantation.

Conclusion

In conclusion, our study has several improvements compared with previous reports. First, dissociated hiPSCs-based NCM culture but not clonal hiPSCs were used to promote iPSC differentiation. Second, hiPSC-RPE cells were enriched by manual curettement and 0.25% EDTA instead of trypsin to reduce the impairment of cell calcium-dependent adhesion. Matrigel and Activin-A treatment were helpful to maintain native RPE functions, such as barrier function, phagocytic activity, and polarized membrane, which were favorable for hiPSC-RPE cell differentiation. Third, the hiPSC-RPE cell spheroids could display less cell senescence and higher cell viability for cell transplantation. Furthermore, supplementation with the ROCK inhibitor Y-27632 in a suspension of hiPSC-RPE cell spheroids for transplantation might favor cell survive in vivo. To summarize, our study suggested that dissociated hiPSCs based on NCM culture were effectively differentiated into transplantable and functional RPE cells through the sequential addition of defined factors but not in the addition of exogenous genes. The hiPSC-RPE cell spheroids maintained adherent monolayer growth on a DCM scaffold in vitro and in the subretina of RPE degenerate chinchilla rabbits in vivo. This study will be beneficial to obtain more native-like RPE cells by spherical culture of RPE cells in order to induce retina regeneration. The preliminary hiPSC-RPE cell spheroids transplantation demonstrates a potential method to treat RPE degenerative diseases.

Abbreviations

RPE:Retinal pigment epithelium; hiPSCs:human induced pluripotent stem cells; NCM:non-colony-type monolayer; RT-PCR:reverse transcription-polymerase chain reaction); TEER:transepithelial electrical resistance; DCM:decellularized corneal matrixes; RP:retinitis pigmentosa; AMD:age-related macular degeneration; ESC:embryonic stem cells; B-CECs:bovine corneal endothelial cells; CSCs:corneal stromal

cells; ADSCs:human adipose-derived stem cells; BM:Bruch's membrane; ECM:acellular extracellular matrix; CECs:corneal epithelial cells; MA:Activin-A; EMT:epithelial-mesenchymal transition.

Declarations

Acknowledgments

This study was supported by the Science Research Grant of Aier Eye Hospital Group, China (AF1601D1).

Author’s contributions

XG and DZ conceived and designed the experiments, performed the experiments, analyzed the data, prepared figures and/or tables approved the final draft. RL, QZ, and SM performed the experiments, approved the final draft. ST and JC conceived and designed the experiments, authored or reviewed drafts of the paper, approved the final draft.

Funding

This work was supported by National Natural Science Foundation of China (No. 81701426 and 81371689), Special Funds for Major Science and Technology Projects of Guangdong Province (2015B010125007), Medical and Health Research Science and Technology Plan Project of Zhejiang Province (2018KY523), and Public Welfare Science and Technology Plan Project of Wenzhou City (Y20180097).

Availability of data and materials

The datasets used and analyzed during the current study are available from the corresponding author on reasonable request.

Ethics approval and consent to participate

Not applicable.

Consent for publication

Not applicable.

Competing interests

The authors declare there are no competing interests.

Author Details

[1]Key Laboratory for Regenerative Medicine, Ministry of Education, Jinan University, Guangzhou, China

[2]Center of Scientific Research, the Second Affiliated Hospital and Yuying Children's Hospital of Wenzhou Medical University, Wenzhou, China

[3]Eye Institute, Medical College of Jinan University, Guangzhou, China

[4]Aier School of Ophthalmology, Central South University, Changsha, China

References

1. Strauss O. The retinal pigment epithelium in visual function. Physiol Rev. 2005;85(3):845-81.
2. Lim LS, Mitchell P, Seddon JM, Holz FG, Wong TY. Age-related macular degeneration. Lancet. 2012;379(9827):1728-38. Epub 2012/05/09. doi: 10.1016/s0140-6736(12)60282-7. PubMed PMID: 22559899.
3. da Cruz L, Chen FK, Ahmado A, Greenwood J, Coffey P. RPE transplantation and its role in retinal disease. Prog Retin Eye Res. 2007;26(6):598-635.
4. Coffey P, Girman S, Wang S, Hetherington L, Keegan D, Adamson P, et al. Long-term preservation of cortically dependent visual function in RCS rats by transplantation. Nat Neurosci. 2002;5(1):53-6.
5. Tezel TH, Del Priore LV, Berger AS, Kaplan HJ. Adult retinal pigment epithelial transplantation in exudative age-related macular degeneration. Am J Ophthalmol. 2007;143(4):584-95. e2.
6. Gabrielian K, Oganesian A, Patel SC, Verp MS, Ernest JT. Cellular response in rabbit eyes after human fetal RPE cell transplantation. Graefes Arch Clin Exp Ophthalmol. 1999;237(4):326-35.
7. Francis PJ, Wang S, Zhang Y, Brown A, Hwang T, McFarland TJ, et al. Subretinal transplantation of forebrain progenitor cells in nonhuman primates: survival and intact retinal function. Invest Ophthalmol Vis Sci. 2009;50(7):3425-31.
8. Inoue Y, Iriyama A, Ueno S, Takahashi H, Kondo M, Tamaki Y, et al. Subretinal transplantation of bone marrow mesenchymal stem cells delays retinal degeneration in the RCS rat model of retinal degeneration. Exp Eye Res. 2007;85(2):234-41.
9. Wang S, Girman S, Lu B, Bischoff N, Holmes T, Shearer R, et al. Long-term vision rescue by human neural progenitors in a rat model of photoreceptor degeneration. Invest Ophthalmol Vis Sci. 2008;49(7):3201-6.
10. Evans MJ, Kaufman MH. Establishment in culture of pluripotential cells from mouse embryos. Nature. 1981;292(5819):154-6.
11. Martin GR. Isolation of a pluripotent cell line from early mouse embryos cultured in medium conditioned by teratocarcinoma stem cells. Proc Natl Acad Sci USA. 1981;78(12):7634-8.
12. Klimanskaya I, Hipp J, Rezai KA, West M, Atala A, Lanza R. Derivation and comparative assessment of retinal pigment epithelium from human embryonic stem cells using transcriptomics. Cloning Stem Cells. 2004;6(3):217-45.
13. Capowski EE, Simonett JM, Clark EM, Wright LS, Howden SE, Wallace KA, et al. Loss of MITF expression during human embryonic stem cell differentiation disrupts retinal pigment epithelium

development and optic vesicle cell proliferation. Hum Mol Genet. 2014:ddu351.

14. Ferguson LR, Balaiya S, Mynampati BK, Sambhav K, Chalam KV. Deprivation of bFGF Promotes Spontaneous Differentiation of Human Embryonic Stem Cells into Retinal Pigment Epithelial Cells. Journal of stem cells. 2015;10(3):159.
15. Zhu Y, Schreiter S, Tanaka EM. Accelerated Three-Dimensional Neuroepithelium Formation from Human Embryonic Stem Cells and Its Use for Quantitative Differentiation to Human Retinal Pigment Epithelium. Methods Mol Biol. 2016:345-55.
16. Takahashi K, Yamanaka S. Induction of pluripotent stem cells from mouse embryonic and adult fibroblast cultures by defined factors. Cell. 2006;126(4):663-76.
17. Yu J, Vodyanik MA, Smuga-Otto K, Antosiewicz-Bourget J, Frane JL, Tian S, et al. Induced pluripotent stem cell lines derived from human somatic cells. Science. 2007;318(5858):1917-20.
18. Iwasaki Y, Sugita S, Mandai M, Yonemura S, Onishi A, Ito S-i, et al. Differentiation/Purification Protocol for Retinal Pigment Epithelium from Mouse Induced Pluripotent Stem Cells as a Research Tool. PLoS One. 2016;11(7):e0158282.
19. Maruotti J, Sripathi SR, Bharti K, Fuller J, Wahlin KJ, Ranganathan V, et al. Small-molecule–directed, efficient generation of retinal pigment epithelium from human pluripotent stem cells. Proc Natl Acad Sci USA. 2015;112(35):10950-5.
20. Maruotti J, Wahlin K, Gorrell D, Bhutto I, Lutty G, Zack DJ. A simple and scalable process for the differentiation of retinal pigment epithelium from human pluripotent stem cells. Stem Cell Transl Med. 2013;2(5):341-54.
21. Chen KG, Mallon BS, Hamilton RS, Kozhich OA, Park K, Hoeppner DJ, et al. Non-colony type monolayer culture of human embryonic stem cells. Stem Cell Res. 2012;9(3):237-48. doi: 10.1016/j.scr.2012.06.003. PubMed PMID: 22910561; PubMed Central PMCID: PMC3490040.
22. Chen KG, Mallon BS, McKay RD, Robey PG. Human pluripotent stem cell culture: considerations for maintenance, expansion, and therapeutics. Cell Stem Cell. 2014;14(1):13-26. doi: 10.1016/j.stem.2013.12.005. PubMed PMID: 24388173; PubMed Central PMCID: PMC3915741.
23. Guo X, Lian R, Guo Y, Liu Q, Ji Q, Chen J. bFGF and Activin A function to promote survival and proliferation of single iPS cells in conditioned half-exchange mTeSR1 medium. Hum Cell. 2015;28(3):122-32. doi: 10.1007/s13577-015-0113-7. PubMed PMID: 25754839.
24. Schwartz SD, Hubschman J-P, Heilwell G, Franco-Cardenas V, Pan CK, Ostrick RM, et al. Embryonic stem cell trials for macular degeneration: a preliminary report. Lancet. 2012;379(9817):713-20.
25. Kamao H, Mandai M, Okamoto S, Sakai N, Suga A, Sugita S, et al. Characterization of human induced pluripotent stem cell-derived retinal pigment epithelium cell sheets aiming for clinical application. Stem cell Rep. 2014;2(2):205-18.
26. Schwartz SD, Regillo CD, Lam BL, Eliott D, Rosenfeld PJ, Gregori NZ, et al. Human embryonic stem cell-derived retinal pigment epithelium in patients with age-related macular degeneration and Stargardt's macular dystrophy: follow-up of two open-label phase 1/2 studies. Lancet.

2015;385(9967):509-16. doi: 10.1016/S0140-6736(14)61376-3. PubMed PMID: WOS:000349213600029.

27. Huang YC, Chan CC, Lin WT, Chiu HY, Tsai RY, Tsai TH, et al. Scalable production of controllable dermal papilla spheroids on PVA surfaces and the effects of spheroid size on hair follicle regeneration. Biomaterials. 2013;34(2):442-51.
28. Bayoussef Z, Dixon JE, Stolnik S, Shakesheff KM. Aggregation promotes cell viability, proliferation, and differentiation in an in vitro model of injection cell therapy. J Tissue Eng Regen Med. 2012;6(10):e61-e73.
29. Guo Y, Liu Q, Yang Y, Guo X, Lian R, Li S, et al. The effects of ROCK inhibitor Y-27632 on injectable spheroids of bovine corneal endothelial cells. Cell Reprogram. 2015;17(1):77-87.
30. Li H, Dai Y, Shu J, Yu R, Guo Y, Chen J. Spheroid cultures promote the stemness of corneal stromal cells. Tissue Cell. 2015;47(1):39-48.
31. Booij JC, Baas DC, Beisekeeva J, Gorgels TG, Bergen AA. The dynamic nature of Bruch's membrane. Prog Retin Eye Res. 2010;29(1):1-18. doi: 10.1016/j.preteyeres.2009.08.003. PubMed PMID: 19747980.
32. Ruberti JW, Zieske JD. Prelude to corneal tissue engineering - gaining control of collagen organization. Prog Retin Eye Res. 2008;27(5):549-77. doi: 10.1016/j.preteyeres.2008.08.001. PubMed PMID: 18775789; PubMed Central PMCID: PMC3712123.
33. da Cruz L, Fynes K, Georgiadis O, Kerby J, Luo YH, Ahmado A, et al. Phase 1 clinical study of an embryonic stem cell-derived retinal pigment epithelium patch in age-related macular degeneration. Nat Biotechnol. 2018;36(4):328-37. doi: 10.1038/nbt.4114. PubMed PMID: 29553577.
34. Davis RJ, Alam NM, Zhao C, Muller C, Saini JS, Blenkinsop TA, et al. The Developmental Stage of Adult Human Stem Cell-Derived Retinal Pigment Epithelium Cells Influences Transplant Efficacy for Vision Rescue. Stem cell Rep. 2017;9(1):42-9. doi: 10.1016/j.stemcr.2017.05.016. PubMed PMID: 28625537; PubMed Central PMCID: PMC5511099.
35. Kashani AH, Lebkowski JS, Rahhal FM, Avery RL, Salehi-Had H, Dang W, et al. A bioengineered retinal pigment epithelial monolayer for advanced, dry age-related macular degeneration. Sci Transl Med. 2018;10(435). doi: 10.1126/scitranslmed.aao4097. PubMed PMID: 29618560.
36. May-Simera HL, Wan Q, Jha BS, Hartford J, Khristov V, Dejene R, et al. Primary Cilium-Mediated Retinal Pigment Epithelium Maturation Is Disrupted in Ciliopathy Patient Cells. Cell Rep. 2018;22(1):189-205. doi: 10.1016/j.celrep.2017.12.038. PubMed PMID: 29298421.
37. Stern JH, Tian Y, Funderburgh J, Pellegrini G, Zhang K, Goldberg JL, et al. Regenerating Eye Tissues to Preserve and Restore Vision. Cell Stem Cell. 2018;22(6):834-49. doi: 10.1016/j.stem.2018.05.013. PubMed PMID: 29859174.
38. Zhao Z, Yu R, Yang J, Liu X, Tan M, Li H, et al. Maxadilan prevents apoptosis in iPS cells and shows no effects on the pluripotent state or karyotype. PLoS One. 2012;7(3):e33953.
39. Maminishkis A, Chen S, Jalickee S, Banzon T, Shi G, Wang FE, et al. Confluent monolayers of cultured human fetal retinal pigment epithelium exhibit morphology and physiology of native tissue. Invest

Ophthalmol Vis Sci. 2006;47(8):3612-24.

40. Guo X, Yu R, Xu Y, Lian R, Yu Y, Cui Z, et al. PAC1R agonist maxadilan enhances hADSC viability and neural differentiation potential. J Cell Mol Med. 2016.
41. Cottin M, Zanvit A. Fluorescein leakage test: a useful tool in ocular safety assessment. Toxicol In Vitro. 1997;11(4):399-405.
42. Guo X, Zhu D, Lian R, Han Y, Guo Y, Li Z, et al. Matrigel and Activin A promote cell-cell contact and anti-apoptotic activity in cultured human retinal pigment epithelium cells. Exp Eye Res. 2016;147:37-49.
43. Cartagena-Rivera AX, Wang W-H, Geahlen RL, Raman A. Fast, multi-frequency, and quantitative nanomechanical mapping of live cells using the atomic force microscope. Sci Rep. 2015;5:11692.
44. Krohne TU, Holz FG, Kopitz J. Apical-to-basolateral transcytosis of photoreceptor outer segments induced by lipid peroxidation products in human retinal pigment epithelial cells. Invest Ophthalmol Vis Sci. 2010;51(1):553-60. doi: 10.1167/iovs.09-3755. PubMed PMID: 19696182.
45. Yang J, Caprioli RM. Matrix sublimation/recrystallization for imaging proteins by mass spectrometry at high spatial resolution. Anal Chem. 2011;83(14):5728-34.
46. Tzameret A, Sher I, Belkin M, Treves AJ, Meir A, Nagler A, et al. Transplantation of human bone marrow mesenchymal stem cells as a thin subretinal layer ameliorates retinal degeneration in a rat model of retinal dystrophy. Exp Eye Res. 2014;118:135-44.
47. Mi X-S, Feng Q, Lo ACY, Chang RC-C, Lin B, Chung SK, et al. Protection of retinal ganglion cells and retinal vasculature by Lycium barbarum polysaccharides in a mouse model of acute ocular hypertension. PLoS One. 2012;7(10):e45469.
48. Greber B, Coulon P, Zhang M, Moritz S, Frank S, Müller-Molina AJ, et al. FGF signalling inhibits neural induction in human embryonic stem cells. The EMBO journal. 2011;30(24):4874-84.
49. Luo Y, Zhuo Y, Fukuhara M, Rizzolo LJ. Effects of culture conditions on heterogeneity and the apical junctional complex of the ARPE-19 cell line. Invest Ophthalmol Vis Sci. 2006;47(8):3644-55.
50. Gamm DM, Melvan JN, Shearer RL, Pinilla I, Sabat G, Svendsen CN, et al. A novel serum-free method for culturing human prenatal retinal pigment epithelial cells. Invest Ophthalmol Vis Sci. 2008;49(2):788-99.
51. Chen FK, Patel PJ, Uppal GS, Tufail A, Coffey PJ, Da Cruz L. Long-term outcomes following full macular translocation surgery in neovascular age-related macular degeneration. Br J Ophthalmol. 2010;94(10):1337-43.
52. Chen FK, Uppal GS, MacLaren RE, Coffey PJ, Rubin GS, Tufail A, et al. Long-term visual and microperimetry outcomes following autologous retinal pigment epithelium choroid graft for neovascular age-related macular degeneration. Clin Experiment Ophthalmol. 2009;37(3):275-85.
53. Hayashi R, Ishikawa Y, Ito M, Kageyama T, Takashiba K, Fujioka T, et al. Generation of corneal epithelial cells from induced pluripotent stem cells derived from human dermal fibroblast and corneal limbal epithelium. PLoS One. 2012;7(9):e45435.

54. Yu D, Chen M, Sun X, Ge J. Differentiation of mouse induced pluripotent stem cells into corneal epithelial-like cells. Cell Biol Int. 2013;37(1):87-94.
55. Abu-Hassan DW, Li X, Ryan EI, Acott TS, Kelley MJ. Induced Pluripotent Stem Cells Restore Function in a Human Cell Loss Model of Open-Angle Glaucoma. Stem Cells. 2015;33(3):751-61.
56. Boucherie C, Mukherjee S, Henckaerts E, Thrasher AJ, Sowden JC, Ali RR. Brief Report: Self-Organizing Neuroepithelium from Human Pluripotent Stem Cells Facilitates Derivation of Photoreceptors. Stem Cells. 2013;31(2):408-14.
57. Parameswaran S, Balasubramanian S, Babai N, Qiu F, Eudy JD, Thoreson WB, et al. Induced Pluripotent Stem Cells Generate Both Retinal Ganglion Cells and Photoreceptors: Therapeutic Implications in Degenerative Changes in Glaucoma and Age-Related Macular Degeneration. Stem Cells. 2010;28(4):695-703.
58. Tucker BA, Park I-H, Qi SD, Klassen HJ, Jiang C, Yao J, et al. Transplantation of adult mouse iPS cell-derived photoreceptor precursors restores retinal structure and function in degenerative mice. PLoS One. 2011;6(4):e18992.
59. Okamoto S, Takahashi M. Induction of retinal pigment epithelial cells from monkey iPS cells. Invest Ophthalmol Vis Sci. 2011;52(12):8785-90.
60. Brandl C, Zimmermann SJ, Milenkovic VM, Rosendahl SM, Grassmann F, Milenkovic A, et al. In-depth characterisation of Retinal Pigment Epithelium (RPE) cells derived from human induced pluripotent stem cells (hiPSC). Neuromolecular Med. 2014;16(3):551-64. doi: 10.1007/s12017-014-8308-8. PubMed PMID: 24801942; PubMed Central PMCID: PMC4119585.
61. Mandai M, Watanabe A, Kurimoto Y, Hirami Y, Morinaga C, Daimon T, et al. Autologous induced stem-cell–derived retinal cells for macular degeneration. N Engl J Med. 2017;376(11):1038-46.
62. Westenskow PD, Bucher F, Bravo S, Kurihara T, Feitelberg D, Paris LP, et al. iPSC-Derived Retinal Pigment Epithelium Allografts Do Not Elicit Detrimental Effects in Rats: A Follow-Up Study. Stem Cells Int. 2016;2016:8470263. doi: 10.1155/2016/8470263. PubMed PMID: 26880994; PubMed Central PMCID: PMC4736415.
63. Buchholz DE, Hikita ST, Rowland TJ, Friedrich AM, Hinman CR, Johnson LV, et al. Derivation of functional retinal pigmented epithelium from induced pluripotent stem cells. Stem Cells. 2009;27(10):2427-34.
64. Carr AJ, Vugler AA, Hikita ST, Lawrence JM, Gias C, Chen LL, et al. Protective effects of human iPS-derived retinal pigment epithelium cell transplantation in the retinal dystrophic rat. PLoS One. 2009;4(12):e8152.
65. Buchholz DE, Pennington BO, Croze RH, Hinman CR, Coffey PJ, Clegg DO. Rapid and efficient directed differentiation of human pluripotent stem cells into retinal pigmented epithelium. Stem cells translational medicine. 2013;2(5):384-93.
66. Menendez L, Kulik MJ, Page AT, Park SS, Lauderdale JD, Cunningham ML, et al. Directed differentiation of human pluripotent cells to neural crest stem cells. Nat Protoc. 2013;8(1):203-12. doi: 10.1038/nprot.2012.156. PubMed PMID: 23288320.

67. McKay BS, Burke JM. Separation of phenotypically distinct subpopulations of cultured human retinal pigment epithelial cells. Exp Cell Res. 1994;213(1):85-92. doi: 10.1006/excr.1994.1176. PubMed PMID: 7517370.
68. Ganti R, Hunt RC, Parapuram SK, Hunt DM. Vitreous modulation of gene expression in low-passage human retinal pigment epithelial cells. Invest Ophthalmol Vis Sci. 2007;48(4):1853-63.
69. Grisanti S, Guidry C. Transdifferentiation of retinal pigment epithelial cells from epithelial to mesenchymal phenotype. Invest Ophthalmol Vis Sci. 1995;36(2):391-405.
70. Lee H, O'Meara SJ, O'Brien C, Kane R. The role of gremlin, a BMP antagonist, and epithelial-to-mesenchymal transition in proliferative vitreoretinopathy. Invest Ophthalmol Vis Sci. 2007;48(9):4291-9.
71. Tamiya S, Liu L, Kaplan HJ. Epithelial-mesenchymal transition and proliferation of retinal pigment epithelial cells initiated upon loss of cell-cell contact. Invest Ophthalmol Vis Sci. 2010;51(5):2755-63.
72. Kokkinaki M, Sahibzada N, Golestaneh N. Human induced pluripotent stem-derived retinal pigment epithelium (RPE) cells exhibit ion transport, membrane potential, polarized vascular endothelial growth factor secretion, and gene expression pattern similar to native RPE. Stem Cells. 2011;29(5):825-35. doi: 10.1002/stem.635. PubMed PMID: 21480547; PubMed Central PMCID: PMCPMC3322554.
73. Page H, Flood P, Reynaud EG. Three-dimensional tissue cultures: current trends and beyond. Cell Tissue Res. 2013;352(1):123-31.
74. Lee WY, Wei HJ, Lin WW, Yeh YC, Hwang SM, Wang JJ, et al. Enhancement of cell retention and functional benefits in myocardial infarction using human amniotic-fluid stem-cell bodies enriched with endogenous ECM. Biomaterials. 2011;32(24):5558-67. Epub 2011/05/11. doi: 10.1016/j.biomaterials.2011.04.031. PubMed PMID: 21555151.
75. Garcion E, Halilagic A, Faissner A. Generation of an environmental niche for neural stem cell development by the extracellular matrix molecule tenascin C. Development. 2004;131(14):3423-32.
76. Jensen UB, Lowell S, Watt FM. The spatial relationship between stem cells and their progeny in the basal layer of human epidermis: a new view based on whole-mount labelling and lineage analysis. Development. 1999;126(11):2409-18.
77. Song X, Zhu C-H, Doan C, Xie T. Germline stem cells anchored by adherens junctions in the Drosophila ovary niches. Science. 2002;296(5574):1855-7.
78. Burridge PW, Thompson S, Millrod MA, Weinberg S, Yuan X, Peters A, et al. A universal system for highly efficient cardiac differentiation of human induced pluripotent stem cells that eliminates interline variability. PLoS One. 2011;6(4):e18293.
79. Lin RZ, Chang HY. Recent advances in three-dimensional multicellular spheroid culture for biomedical research. Biotechnol J. 2008;3(9-10):1172-84.
80. Mimura T, Yamagami S, Yokoo S, Usui T, Amano S. Selective isolation of young cells from human corneal endothelium by the sphere-forming assay. Tissue Eng Part C Methods. 2010;16(4):803-12. doi: 10.1089/ten.TEC.2009.0608. PubMed PMID: 19852617.

81. Cheng NC, Chen SY, Li JR, Young TH. Short-term spheroid formation enhances the regenerative capacity of adipose-derived stem cells by promoting stemness, angiogenesis, and chemotaxis. Stem Cells Transl Med. 2013;2(8):584-94. doi: 10.5966/sctm.2013-0007. PubMed PMID: 23847001; PubMed Central PMCID: PMC3726138.
82. Ranaei Pirmardan E, Soheili ZS, Samiei S, Ahmadieh H, Mowla SJ, Ezzati R, et al. Characterization of a spontaneously generated murine retinal pigmented epithelium cell line; a model for in vitro experiments. Exp Cell Res. 2016;347(2):332-8. doi: 10.1016/j.yexcr.2016.08.015. PubMed PMID: 27554602.
83. Bi YL, Zhou Q, Du F, Wu MF, Xu GT, Sui GQ. Regulation of functional corneal endothelial cells isolated from sphere colonies by Rho-associated protein kinase inhibitor. Exp Ther Med. 2013;5(2):433-7. doi: 10.3892/etm.2012.816. PubMed PMID: 23408756; PubMed Central PMCID: PMC3570180.
84. Zhang L, Valdez JM, Zhang B, Wei L, Chang J, Xin L. ROCK inhibitor Y-27632 suppresses dissociation-induced apoptosis of murine prostate stem/progenitor cells and increases their cloning efficiency. PLoS One. 2011;6(3):e18271. doi: 10.1371/journal.pone.0018271. PubMed PMID: 21464902; PubMed Central PMCID: PMC3065488.
85. Wongpichedchai S, Weiter JJ, Weber P, Dorey CK. Comparison of external and internal approaches for transplantation of autologous retinal pigment epithelium. Invest Ophthalmol Vis Sci. 1992;33(12):3341-52. PubMed PMID: 1428708.
86. Wang H, Leonard DS, Castellarin AA, Tsukahara I, Ninomiya Y, Yagi F, et al. Short-term study of allogeneic retinal pigment epithelium transplants onto debrided Bruch's membrane. Invest Ophthalmol Vis Sci. 2001;42(12):2990-9. Epub 2001/11/01. PubMed PMID: 11687547.
87. Gouras P, Tanabe T. Survival and integration of neural retinal transplants in rd mice. Graefes Arch Clin Exp Ophthalmol. 2003;241(5):403-9. doi: 10.1007/s00417-003-0648-2. PubMed PMID: 12698256.

Supplemental Figure Legends

Figure S1 The condition of dissociated hiPSCs based on Non-colony-type Monolayer (NCM) culture compared with clonal hiPSCs. (A) Immunofluorescence examining protein expression in dissociated hiPSCs and clonal hiPSCs. (B) RT-PCR analysis of gene expression in dissociated hiPSCs and clonal hiPSCs. (C). qPCR analysis mRNA expression levels in dissociated hiPSCs and clonal hiPSCs.

Figure S2 The karyotype condition of dissociated hiPSCs based on Non-colony-type Monolayer (NCM) culture compared with clonal hiPSCs. (A) Karyotype analysis of dissociated hiPSCs. (B) Karyotype analysis of clonal hiPSCs.

Figue S3 The morphology of hiPSC, hiPSC-RPE, and hRPE cells using AFM. (A) 2D and 3D AFM images of hiPSC, hiPSC-RPE, and hRPE cells of the cell, cell surface, and cell nucleus. (B) Statistical comparison of cell length, width, and height in hiPSC, hiPSC-RPE, and hRPE cells. (C) Statistical comparison of nuclei length, width, and height in hiPSC, hiPSC-RPE, and hRPE cells. A difference with $^{*}P<0.05$ was considered

statistically significant. A difference with $^{\#}P>0.05$ was considered not statistically significant. Bars represent mean ± SEM, n=3.

Figure S4 Injectability of the hiPSC-RPE cell spheroids. (A) Preparation of porcine lamellar corneal matrix (100 μm thickness) using a microkeratome. (B) The frozen sections of cellularized and decellularized corneal matrix stained with DAPI and H&E. (C) The process of hiPSC-RPE cell spheroid generation.

Figure S5 Injectability of hiPSC-RPE cell spheroids *in vivo*. (A) hiPSC-RPE cell spheroids were labeled with PKH26. (B) The external approach transplantation of hiPSC-RPE cell spheroids into the subretina space of chinchilla rabbits (arrow represents the transplantation position). (C) A schematic diagram of the external approach to transplantation of hiPSC-RPE cell spheroids into the subretina.

Tables

Table 1. Primer information

Primers	Sequences (5'to 3')	Product length	GeneBank Number
GADPH-F	CCACTAGGCGCTCACTGTTC	180bp	NM_001289746.1
GADPH-R	TTGAGGTCAATGAAGGGGTCA		
RPE-65-F	TGACCGATTCAAGCCATCTT	363bp	NM_000329.2
RPE-65-R	ACCTCTTCCCAGTTCTCACG		
Otx2-F	GGAAGGGAGGGAAGGTCATA	343bp	NM_001270523.1
Otx2-R	GCAGAGGTGGAGTTCAAGGT		
EMMPRIN-F	GCAGGTTCTTCGTGAGTTCC	314bp	NM_001728.3
EMMPRIN-R	GCCTTTGTCATTCTGGTGCT		
CRALBP-F	AAGCCATCCACTTCATCCAC	338bp	NM_000326.4
CRALBP-R	TCTCAAGCAGCCCTTTCCTA		
Nanog-F	CAAGAACTCTCCAACATCCTGAA	126bp	NM_024865.2
Nanog-R	CCTGCGTCACACCATTGCTATTC		
Oct4-F	GAAGGATGTGGTCCGAGTGT	183bp	NM_001173531.2
Oct4-R	GTGAAGTGAGGGCTCCCATA		
Sox2-F	CAGGAGTTGTCAAGGCAGAGA	171bp	NM_003106.3
Sox2-R	CCGCCGCCGATGATTGTTA		
Klf4-F	GCCGCTCCATTACCAAGAG	166bp	NM_004235.4
Klf4-R	GTGTGCCTTGAGATGGGAAC		
c-Myc-F	CATCAGCACAACTACGCAGC	120bp	NM_002467.4
c-Myc-R	GCTGGTGCATTTTCGGTTGT		
Lin28-F	CCCATCACTGGGGTGTGTTT	162bp	NM_024674.4
Lin28-R	CAGTTTGCGTACCAATAAGTCTTT		
Nestin-F	AACAGCGACGGAGGTCTCTA	220bp	NM_006617.1
Nestin-R	TTCTCTTGTCCCGCAGACTT		
Pax6-F	TGTTGCGGAGTGATTAGTGGG	196bp	NM_000280.4
Pax6-R	TTGGTGATGGCTCAAGTGTGT		

Table 2. Antibodies

Antibody	Species	Vendor (City, State, catalogue)	Dilution				
			WB	IC	FC	IF	
b-ACTIN	mouse	Santa Cruz (Santa Cruz, CA, sc-47778)	1:1000	ND		ND	ND
CRALBP	mouse	Abcam (Cambridge, MA, ab15051)	1:5000	ND		1:100	1:350
Mitf	rabbit	Abcam (Cambridge, MA, ab122982)	1:10000	ND		1:100	1:1000
Tyrosinase	rabbit	Abcam (Cambridge, MA, ab180753)	1:5000	ND		ND	1:100
Otx2	mouse	Abcam (Cambridge, MA,, ab130238)	1:5000	ND		ND	1:500
EMMPRIN	mouse	Abcam (Cambridge, MA, ab119114)	1:3000	ND		1:100	1:100
RPE-65	mouse	Abcam (Cambridge, MA, ab13826)	1:10000	ND		1:100	1:1000
Nanog	rabbit	Cell Signaling (Danvers, MA, 8822)	1:1000	ND		ND	1:500
Oct4	rabbit	Cell Signaling (Danvers, MA, 2750)	1:1000	ND		1:100	1:100
Sox2	rabbit	Cell Signaling (Danvers, MA, 3579)	1:1000	ND		1:100	1:100
Klf4	rabbit	Cell Signaling (Danvers, MA, 12173)	1:1000	ND		ND	ND
SSEA4	mouse	Cell Signaling (Danvers, MA, 4755)	ND	ND		ND	1:500
TRA-1-60	mouse		ND	ND		ND	1:500

ZO-1	mouse	Cell Signaling (San Francisco, CA, 4746)	ND	ND	ND	1:500
Occludin	rabbit	BD (San Diego, CA, 610967)	ND	ND	ND	1:100
Nestin	mouse	Bioss (Shanghai, ab16287)	1:1000	ND	ND	ND
AHNA	mouse	Santa Cruz (Santa Cruz, CA, sc-23927)	ND	1:400	ND	ND
GADPH	rabbit	Abcam (Cambridge, MA, ab191181) Bioworld (Louis , MN, AP0063)	1:3000	ND	ND	ND

ND = Not detected; WB = Western blot; IC = Immunohistochemistry; FC = Flow Cyt; IF = Immunofluorescence.

Figures

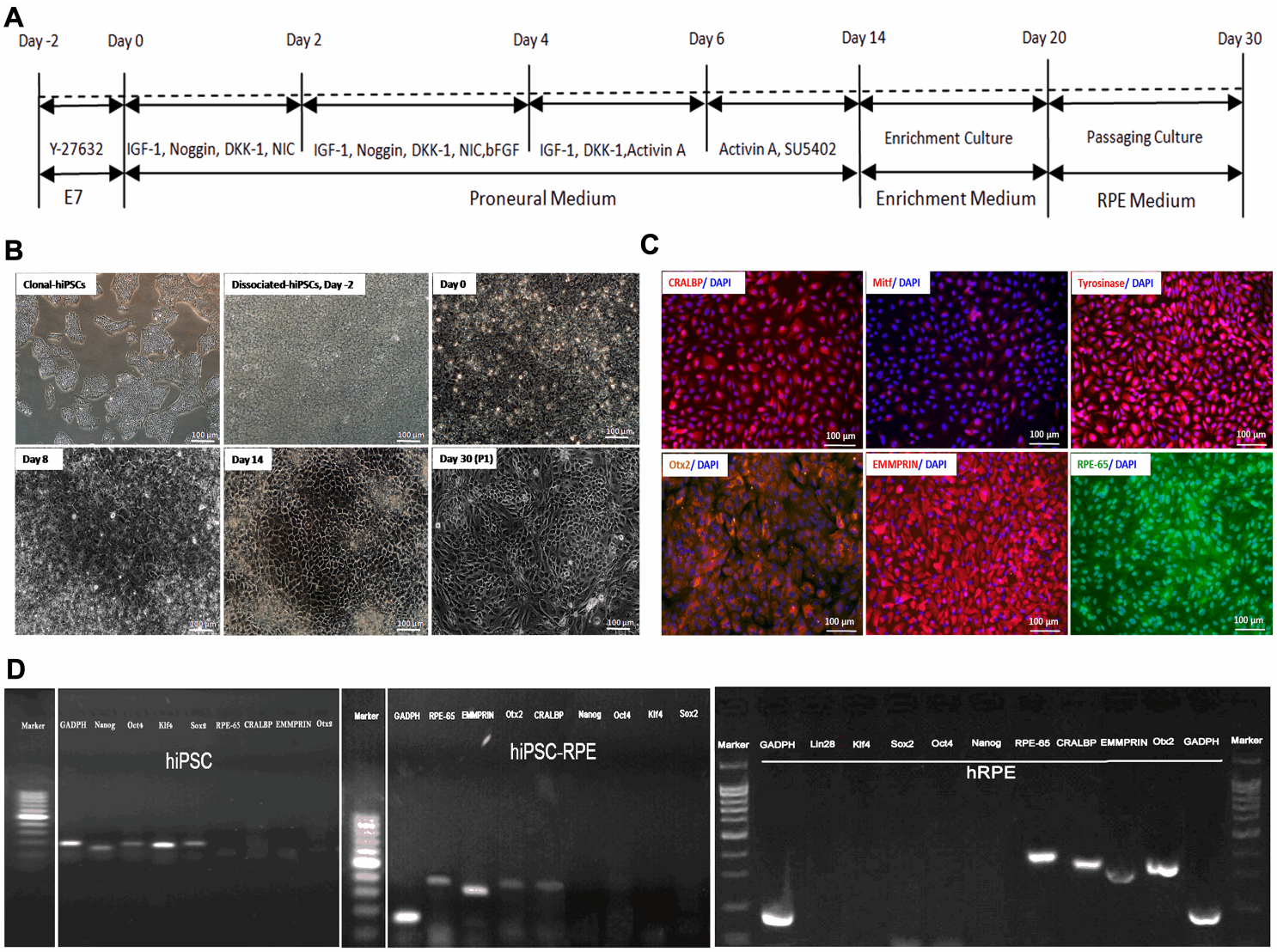

Figure 1

Differentiation and identification of hiPSC-RPE cells. (A) A schematic illustration of the differentiation protocol of the hiPSC-RPE cells. (B) Morphological changes in the differentiation of cells under an inverted microscope. (C) The identification of hiPSC-RPE cells (P1) using an immunofluorescence assay and (D) an RT-PCR assay.

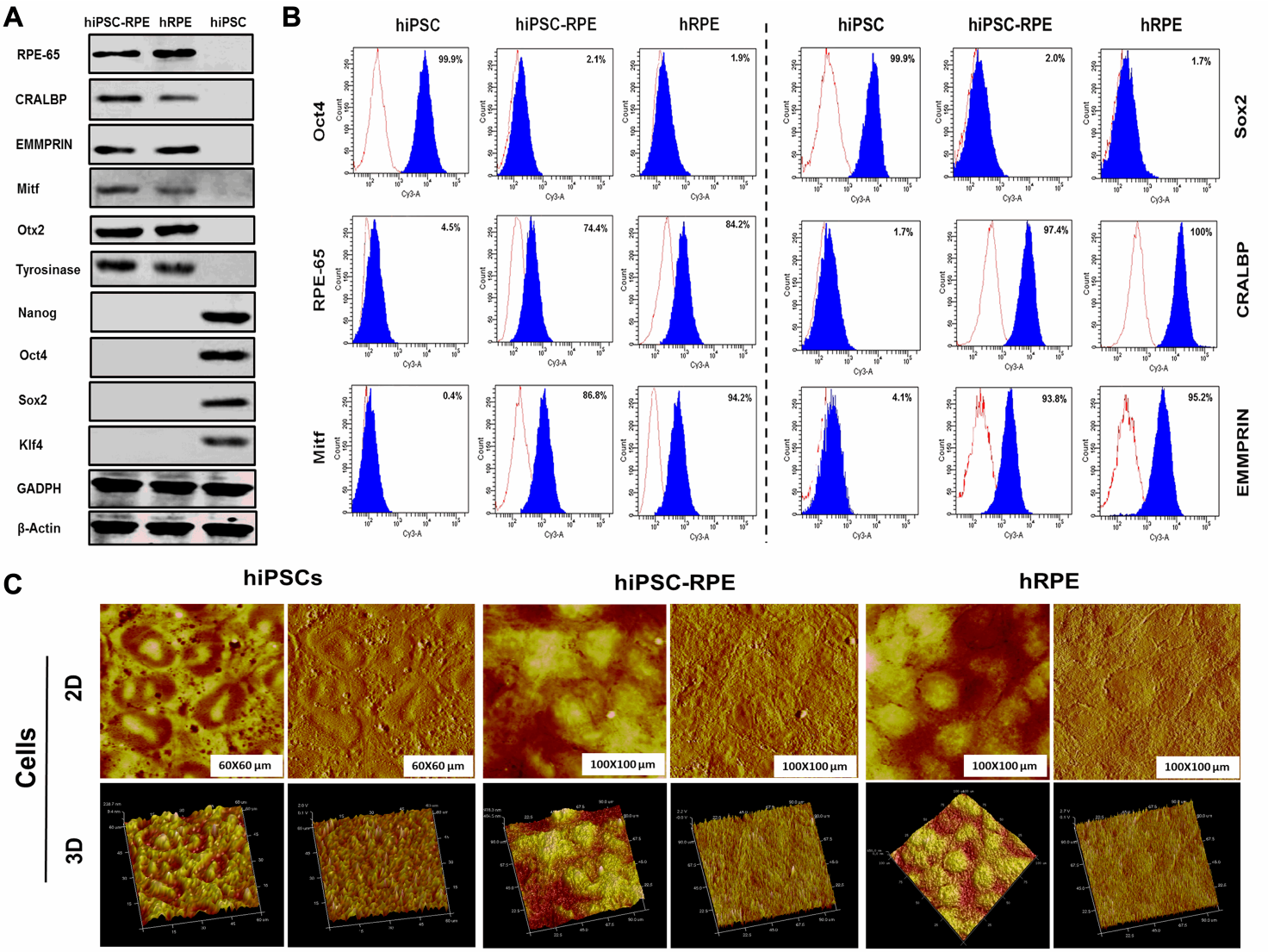

Figure 2

Further identification of hiPSC-RPE cells. (A) Identification of hiPSC-RPE cells (P1) using western blotting. (B) Representative flow cytometry histograms of hiPSC, hiPSC-RPE (P1), and hRPE cells. (C) 2D and 3D topography images of hiPSC, hiPSC-RPE (P1), and hRPE cells by AFM.

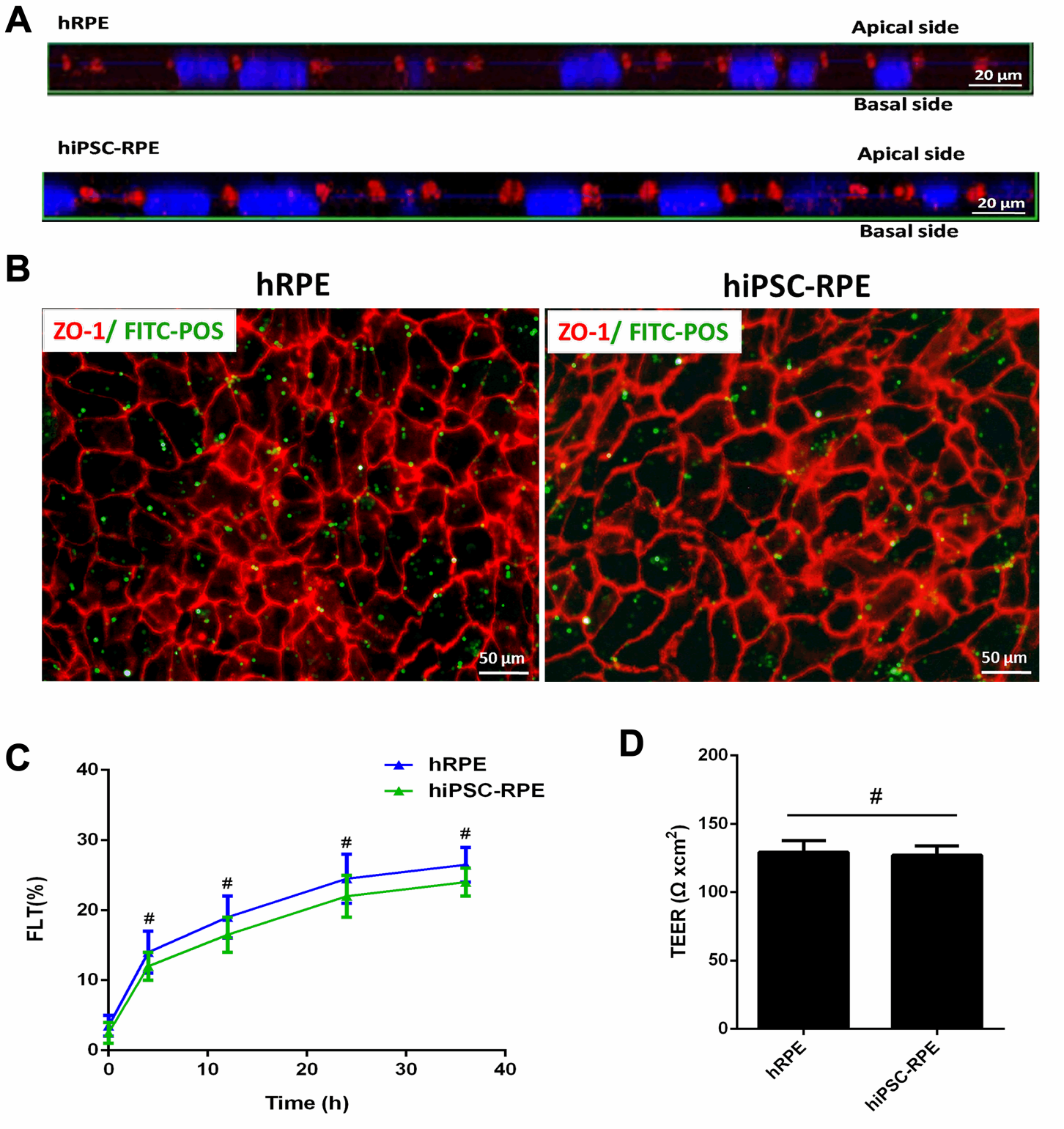

Figure 3

Identification of RPE-like function in hiPSC-RPE cells. (A) A Z-stack confocal micrograph showing typical polarized expression of ZO-1 demonstrated apical localization in hRPE and hiPSC-RPE cells. (B) The phagocytosis of FITC-POS and ZO-1 staining in hRPE and hiPSC-RPE cells. (C) The comparison of a dynamic barrier of hRPE and hiPSC-RPE cells through a fluorescein leakage test at 0, 4, 12, 24, and 36 h.

(D) TEER assay assesses the dynamic barrier function in hRPE and hiPSC-RPE cells. Differences with #P>0.05 (hRPE vs hiPSC-RPE) were considered not significant. Bars represent mean ± SEM, n=3.

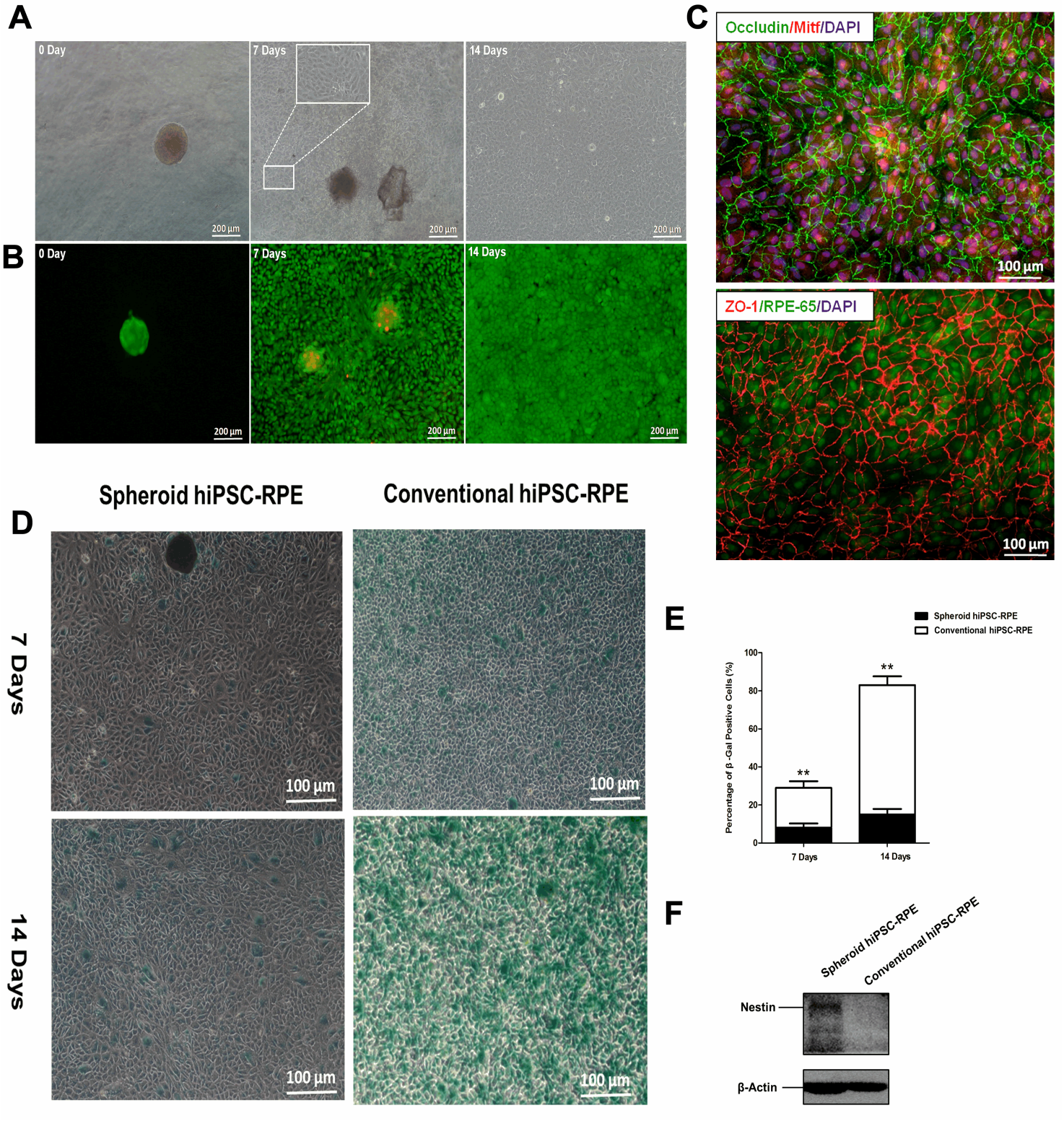

Figure 4

Seeding hiPSC-RPE cell spheroids on DCM. (A) Brightfield images of hiPSC-RPE cell spheroids on DCM on day 0, 7, and 14. (B) Calcein AM and EthD-III double staining of hiPSC-RPE cell spheroids on DCM on day 0, 7, and 14. (C) The double staining of Occludin and Mitf or ZO-1 and RPE-65 in hiPSC-RPE cell

spheroids on DCM on day 14. (D) Detection of SA-β-Gal activity in spheroid or conventional culture hiPSC-RPE cells on days 7 and 14. (E) Quantification of SA-β-Gal activity with ImageJ software. (F) The expression of Nestin in spheroid or conventional culture hiPSC-RPE cells on day 14. A difference with **P<0.01 (spheroid culture hiPSC-RPE vs conventional culture hiPSC-RPE on day 7 and 14) was considered statistically significant. Bars represent mean ± SEM, n=3.

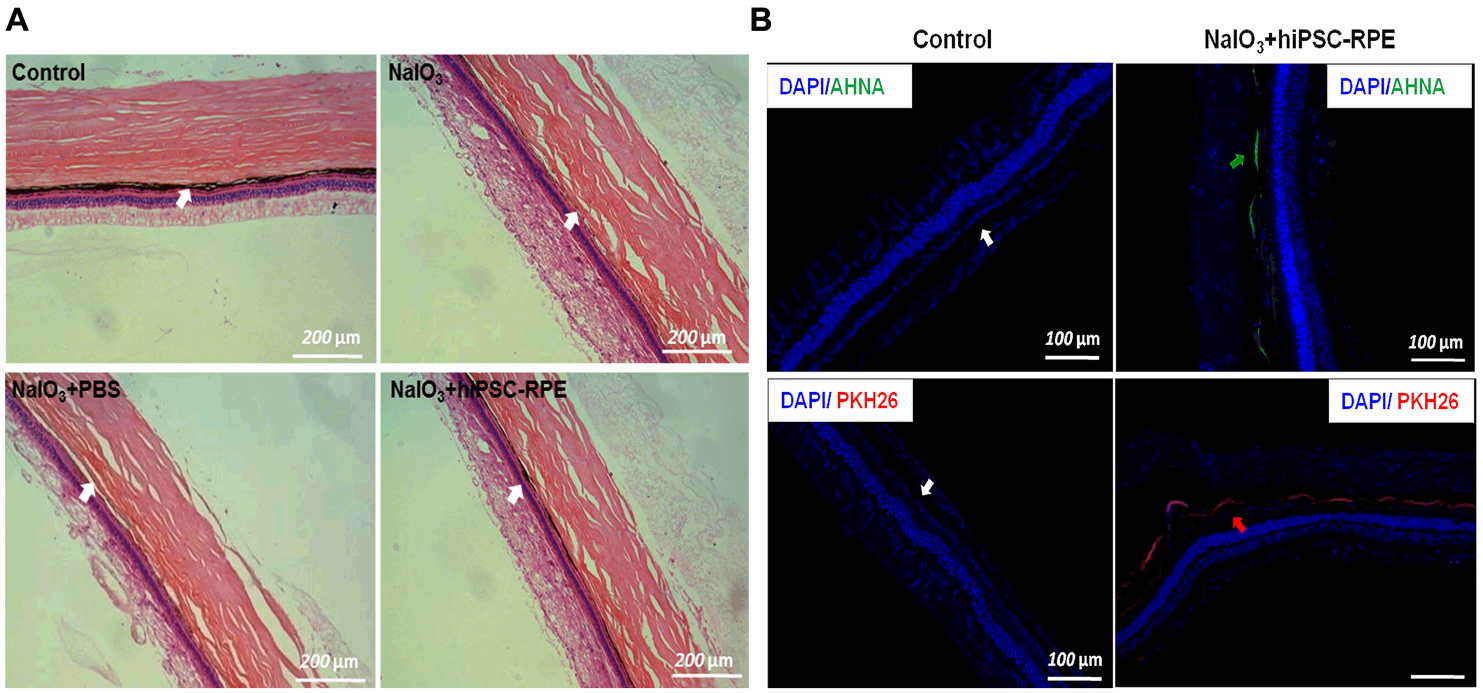

Figure 5

Injectability of hiPSC-RPE cell spheroids in vivo. (A) H&E-staining of paraffin sections after one month of hiPSC-RPE cell spheroid injection in vivo (arrows represent RPE layer). (B) Immunohistochemistry of paraffin sections after one month of hiPSC-RPE cell spheroid injection in vivo (white arrow represents RPE layer in control; green arrow represents AHNA positive of partial hiPSC-RPE cell sheets in NaIO3+hiPSC-RPE; red arrow represents partial hiPSC-RPE cell sheets labeled PKH26 in NaIO3+hiPSC-RPE).

Supplementary Files

This is a list of supplementary files associated with this preprint. Click to download.

- FigureS2.tif
- FigureS1.tif
- FigureS3.tif
- FigureS4.tif
- FigureS5.tif